Available online at www.sciencedirect.com
SCIENCE DIRECT®
Journal of Power Sources 118 (2003) 276–285
JOURNAL OF POWER SOURCES
www.elsevier.com/locate/jpowsour

$LaCrO_3$-based anodes: stability considerations

Joseph Sfeir[*,1]

Laboratory of Photonics and Interfaces, Swiss Federal Institute of Technology, EPFL, CH-1015 Lausanne, Switzerland

Abstract

$LaCrO_3$ based materials have been studied as alternative anodes to the conventional Ni-YSZ cermet. Thermodynamic calculations as well as experimental work have been conducted in an attempt to analyze the stability of this system when doped with Mg, Ca, Sr, Mn, Fe, Co and Ni. Various gas atmospheres were simulated (air, humidified hydrogen, CO and CO_2). It was possible to correlate some of the experimental results (electrochemical, *XRD*, *XPS-Auger*, *SIMS* and *TEM-EDS*) with the thermodynamic calculations. It was calculated that Sr and Mn substitution maintain the stability of the perovskite even in the severe reducing conditions used in SOFC, whereas the other substitutions destabilize the system. Experimentally, transition metal substituted $LaCrO_3$ did not decompose readily in the reducing atmospheres containing wet hydrogen or methane indicating that the demixing is at least kinetically hindered.

Keywords: SOFC; Anode; Lanthanum chromite $LaCrO_3$; Thermodynamic calculation; Effect of substituents; Effect of corrosive gases

1. Introduction

In solid oxide fuel cells (SOFC), lanthanum chromites, $LaCrO_3$, were investigated for their use as interconnect materials for cell stacking and potentially as cathode [1] and anode [2] electrocatalysts. These perovskite materials are reported to be quite stable in both oxidative and reductive atmospheres [3]. They can be easily substituted on the *A* and *B* sites with alkali earth and transition metal elements respectively, which allows interesting modifications of their electronic as well as their catalytic properties [4]. In literature, many reports focus on the doping effect of alkali earth (Mg, Ca, Sr) as well as transition metal (Co, Ni, Cu) elements on the conductivity, sintering and stability behavior of these materials. Less work is however done on catalysis, electrocatalysis and the effect of corrosive gases.

We previously explored calcium and/or strontium and magnesium substituted lanthanum chromites as alternative anodes to Ni-YSZ cermet [5]. These materials were observed to inhibit coking but their overall electrocatalytic activity was found to be low under pure methane feed. Also, a small degradation was observed and was related to a progressive reduction of the electrode as well as a topotactic reaction between excess Ca or Sr with YSZ. It was also found that part of this degradation could originate from an electrochemical demixing effect [6]. This reaction was however reduced when low substitution levels were adopted (around 15% on the *A*-site). Characterization measurements done on powders of different compositions subjected to methane rich atmospheres during catalytic measurements, showed surface enrichments of Sr and Ca following the exposure to particular gases [7]. Further improvements were undertaken following these results and stable anode materials for the direct CH_4 feed were obtained [8]. In the present study, a chemical thermodynamic analysis was undertaken in the perspective of understanding the stability, the solubility limit of substituents as well as the effect of oxidative, reductive and corrosive gases (air, wet hydrogen, CO and CO_2) on (Mg, Ca, Sr, Mn, Fe, Co, Ni)-substituted $LaCrO_3$. Trials were made to correlate these estimations with experimental results based on electrochemical, *XRD*, *SEM*, *SIMS*, *XPS-Auger* and *TEM-EDS* characterizations.

2. Estimating thermodynamic properties

The thermodynamic data for most of the different substituted $LaCrO_3$ species used in this study are not available in the literature so that the thermodynamic parameters for these phases had to be estimated. For that purpose, the different $LaCrO_3$ phases were treated as ideal solid solutions of $LaCrO_3$ and $MCrO_3$, and $LaCrO_3$ and $LaCr_{0.5}M_{0.5}O_3$ for the *A*-site and *B*-site *M*-substituents respectively, following a

* Tel.: +41-76-415-5905; fax: +41-21-634-5905.
E-mail address: joseph.sfeir@epfl.ch (J. Sfeir).
[1] Present address: HTceramix SA, EPFL Science Park, PSE-C, Swiss Federal Institute of Technology, EPFL, CH-1015 Lausanne, Switzerland.

0378-7753/03/$ – see front matter
doi:10.1016/S0378-7753(03)00099-5

procedure developed by Yokokawa et al. [9–11]. The molar Gibbs free energy for the ideal solid solution was taken as:

$$G_{\text{perovskite}} = \sum x_i \Delta_f G_i^\circ + RT \sum x_i \ln(x_i) \quad (1)$$

where x_i is the mole fraction of species i in the solution, $\Delta_f G_i^\circ$ the standard Gibbs free energy of formation of species i, and R the gas constant. The standard entropy of the perovskite oxides was derived from the following expression:

$$\Delta_r S_{298}^\circ = 10\,\text{J/mol}\,K = S_{298,\,\text{perovskite}}^\circ - \sum x_i S_{298,\,\text{binary oxide}}^\circ \quad (2)$$

where $\Delta_r S_{298}^\circ$ was set to 10 J/mol K according to Yokokawa et al. [9], the binary oxides stand for the La_2O_3, Cr_2O_3 and the other element oxides by supposing the following kind of reaction:

$$\frac{1}{2}La_2O_3 + \frac{1}{2}Cr_2O_3 = LaCrO_3 \quad (3)$$

The heat capacity coefficients were estimated using:

$$\alpha_{\text{perovskite}} = \sum x_i \alpha_{\text{binary oxide}} \quad (4)$$

Also, in order to estimate the enthalpy of formation $\Delta_f H_{298}^\circ$ of the $LaCr_{0.5}M_{0.5}O_3$, $LaCr_{0.5}M_{0.5}O_{2.75}$ and $LaM_{0.5}Cr_{0.5}O_{2.75}$ phases, the correlation relating the stabilzation energy, ∂, to $\Delta_f H_{298}^\circ$ and the tolerance factor (Goldschmid), t_p, derived by Yokokawa et al. [9] was used:

$$\partial[\text{kJ/mol}] = -90 + 720(1 - t_p) = \Delta_f H_{298,\,\text{perovskite}}^\circ - \sum x_i \Delta_f H_{298,\,\text{binary oxide}}^\circ \quad (5)$$

and,

$$t_p = \frac{r_O + r_A}{\sqrt{2}(r_O + r_B)} \quad (6)$$

with r_O, r_A and r_B the mean Shannon ionic radii [12] of the O, A and B sites, respectively. The transition metal substituents were taken in the low spin state. The difference with a high spin state is at most of 1.5%.

The non-stoichiometry, δ, was taken into account by treating the non-stoichiometric compounds as ideal solid solutions of $LaCrO_3$ and $LaM_{0.5}Cr_{0.5}O_{2.75}$ or $LaCr_{0.5}M_{0.5}O_{2.75}$ for the A-site and B-site M-substituents, respectively. In the case of Ca and Sr substitutions, the thermodynamic data for $LaM_{0.5}Cr_{0.5}O_{2.95}$ were corrected by using the experimental K_{ox} published by Yasuda et al. [13] and Peck et al. [14] from:

$$\Delta_f G_{La_{1-x}(Ca,\,Sr)_xCrO_3,\,T}^\circ = \Delta_f G_{La_{1-x}(Ca,\,Sr)_xCrO_{3-\delta},\,T} + \delta \Delta_{\text{ox}} G_T^\circ \quad (7)$$

and,

$$\ln K_{\text{ox}} = -\frac{\Delta_{\text{ox}} H^\circ}{RT} + \frac{\Delta_{\text{ox}} S^\circ}{R} \quad (8)$$

The evolution of K_{ox} for Ca substitution was extrapolated from Yasuda et al.'s thermogravimetric data [13] using the same slope for the x dependency of $\Delta_{\text{ox}} H^\circ$ and $\Delta_{\text{ox}} S^\circ$ as for the Sr substitution given by Peck et al. [14]. For Mg substitution the value given by van Dieten was used [10]. For the other substituents, no experimental data for K_{ox} nor non-stoichiometry data were available in literature so that no correction was possible.

The thermodynamic equilibrium calculations were made using the HSC-4.1, thermodynamic equilibria calculation software, from Outokumpu Research Oy, Finland, using the thermodynamic data delivered in the software package as well as thermodynamic data obtained from literature [9,10,14,15] and other laboratories. The different species taken into account for these calculations are listed in the Appendix A. Neither melts or mixed Ruddlesden–Popper phases nor hydroxylapatite-like oxides were taken into account. These compounds were however reported to coexist with the $LaCrO_3$-based perovskites [16–21].

3. Results

The summary of the thermodynamic data thus generated and used for the following calculations is given in Appendix B.

3.1. Air solubility limit estimations for Ca and Sr extrapolated from experimental data

The experimental solubility limit, x, for Sr in $LaCrO_3$ is reported to be 0.1 and 0.31 at 950 °C in air and 1600 °C in 10^{-9} atm of oxygen respectively [14,22], 0.1 at 1100 °C [23], or 0.07 at 650 °C in air [24]. For Ca, the solubility limit in air is 0.15 at 800 °C [6], 0.31 and 0.22 at 950 °C in air and at 1600 °C in 10^{-9} atm of oxygen respectively [21], 0.12 at 650 °C in air [24], and 0.2, 0.3 and 0.4 at 900, 1000 and 1030 °C in air respectively [25]. This correlates well with the data recently published by Miyoshi et al. [23].

Furthermore, the main secondary phase which experimentally coexists, at low temperatures (~1200 °C), with the $La_{1-x}Sr_xCrO_3$ perovskite phase is $SrCrO_4$, with small amounts of other phases such as $Sr_{2.67}Cr_2O_8$ and $La_{16}Cr_7O_{44}$ [14,20,23,24,26]. For the case of Ca, it is reported that $CaCrO_4$ forms predominantly [6,21,23–25,27]. Also, we [7] observed by *TEM* a $CaCrO_4$ secondary phase on high Ca substituted $LaCrO_3$. The origin of the difference in the minor secondary phases composition reported in literature was partly rationalized by Chick et al. [27].

Based on these results, $La_{1-x}(Ca, Sr)_xCrO_3$ phases were assumed to be formed as an ideal solution between $LaCrO_3$ and $(Ca, Sr)CrO_3$. From the 'symmetrical regular solutions model' [28,29] we have for the $(A, B)_nO$ system:

$$G_{\text{ss}} = \underbrace{(x_A \mu_{A_nO}^\circ + x_B \mu_{B_nO}^\circ)}_{G^\circ} + \underbrace{\{nRT(x_A \ln x_A + x_B \ln x_B)\}}_{G_{\text{mix}}} + \underbrace{(nx_A x_B W_G)}_{GX_S} \quad (9)$$

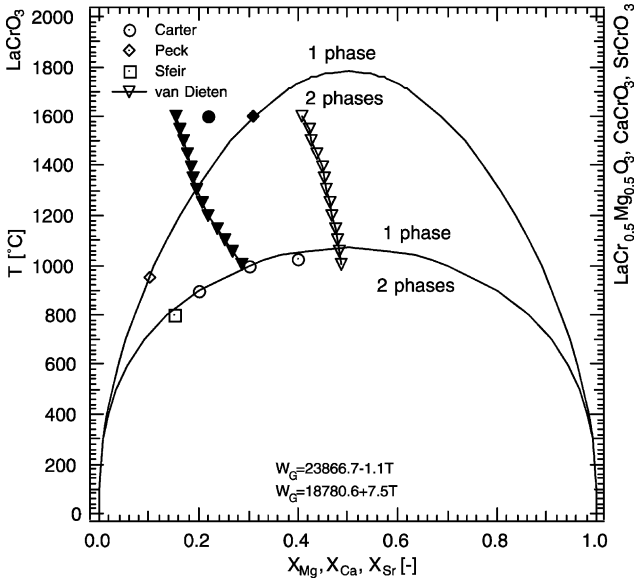

Fig. 1. The solubility limit of $La_{1-x}Ca_xCrO_3$ and $La_{1-x}Sr_xCrO_3$ as extrapolated from experimental results [6,14,25] using the 'symmetrical regular solutions model'. The solubility limit of Mg [10] is also given to illustrate the case of a *B*-site substitution which does not follow the regular model. (○) and (▽) open symbols refer to air whereas (●) and (▼) solid symbols refer to a low oxygen partial pressure of about 10^{-8} atm for Mg and Ca, respectively. It is observed that for Ca [21] and Mg [10], the solubility limit decrease in reducing conditions. Sr [20] does not seem to be affected.

with, G_{ss} the molar free energy of solution, x_A mole fraction of A_nO and x_B mole fraction of B_nO ($x_A + x_B = 1$) and $W_G = W_{H,1\,bar} - TW_S$, the interaction parameter (no ordering or clustering of atoms is assumed). The evolution of x with temperature is then given by:

$$\ln\left(\frac{x}{1-x}\right) = \frac{W_G}{RT}(2x-1) \tag{10}$$

This allows the estimation of W_G from the experimental data and the plot of the expected solubility limit for Ca and Sr in function of temperature as shown in Fig. 1.

3.2. Stability in high oxygen partial pressures for (Ca, Sr) substituted $LaCrO_3$

$La_{1-x}Ca_xCrO_3$ and $La_{1-x}Sr_xCrO_3$ stability, as calculated from our estimates, under high oxygen partial pressures is depicted in Fig. 2 as a function of x. The reaction equations shown here were chosen among others because they depict the easiest reaction path. In air, the stability region with Ca is wider than with Sr. The solubility of Sr under oxygen, calculated at 800 °C, lies near 0.07, as expected from the extrapolated value taken from Fig. 1. Ca substitution, however, seems to be more favourable in our calculations than reported in literature. The thermodynamic parameters estimated for $La_{1-x}Ca_xCrO_3$ are such that the species have become too stable. However, no attempt was undertaken to adjust these parameters.

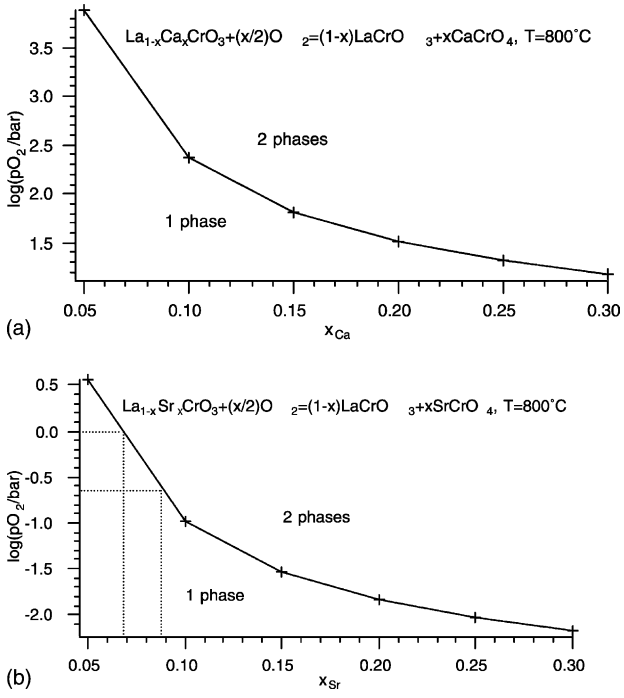

Fig. 2. $La_{1-x}Ca_xCrO_3$ and $La_{1-x}Sr_xCrO_3$ stability at 800 °C, under high oxygen partial pressures as a function of x.

3.3. Stability in low oxygen partial pressures for (Ca, Sr) substituted $LaCrO_3$

Fig. 3 shows the stability of $La_{1-x}Ca_xCrO_3$ and $La_{1-x}Sr_xCrO_3$, as a function of x, under low oxygen partial pressures corresponding to the working atmosphere of an anode in 3% $H_2O + H_2$ or CH_4. These calculations indicate that, for the *A*-site substitution, Ca would highly destabilize the $LaCrO_3$ phase whereas Sr would be expected to preserve the perovskite phase even under the lowest oxygen partial pressures encountered on the anode side. It is only at the highest temperature (1000 °C) that Ca-containing species enters the stability region in contact with humidified H_2. The lower solubility limit of calcium under low oxygen partial pressure is also observed experimentally at 1600 °C, in 10^{-9} atm by Peck et al. [21], whereas Sr solubility is reported to increase in low P_{O_2} [22]. Thus, the Sr substitution could be more appropriate than Ca for an anode purpose.

3.4. Volatility diagrams: effect of the gas composition for (Ca, Sr) substituted $LaCrO_3$

Fig. 4 shows the volatility diagrams of $LaCrO_3$, $La_{0.85}Ca_{0.15}CrO_3$ and $La_{0.93}Sr_{0.07}CrO_3$ systems, at 800 °C. These were drawn following the procedure described by Lou et al. [30,31], and by piling up different diagrams. These diagrams were set up by generating ≈1200 reactions for both Sr and Ca substitutions, by checking the thermodynamic stability of each phase combination and deriving valid

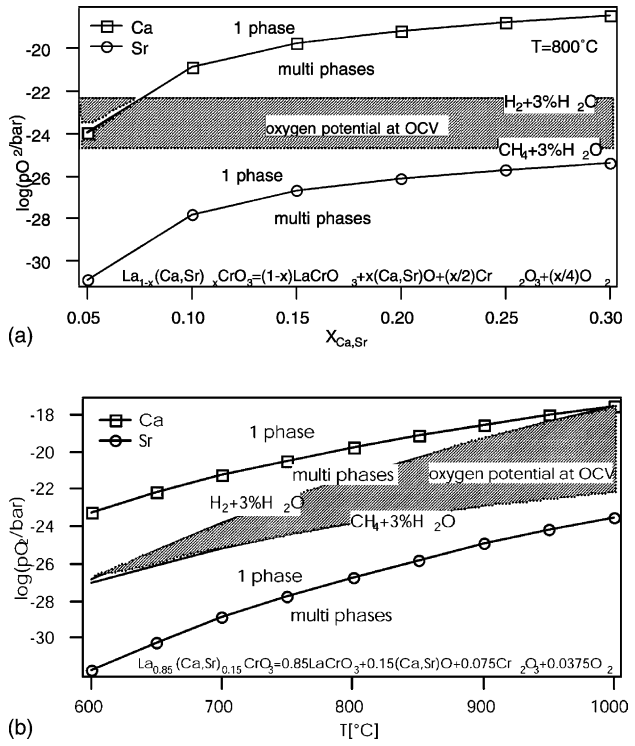

Fig. 3. $La_{1-x}Ca_xCrO_3$ and $La_{1-x}Sr_xCrO_3$ stability under low oxygen partial pressures as a function of x, at 800 °C, and the effect of temperature on $x = 0.15$.

phase relations. The chemical reactivity of the materials is determined by the behavior of the most reactive components. The substitution level of $x = 0.15$ and 0.07 for Ca and Sr respectively was chosen based on the solubility limit at 800 °C in air as extrapolated from Fig. 1. From these diagrams, it is clearly observed that the stability region of $LaCrO_3$ is modified by substitution with Ca and Sr, as discussed above. In reducing atmospheres, Ca substitution is expected to be less favourable than Sr. The stability domain of the different species is expressed as bold lines and given as a function of the oxygen partial pressure. Further, these diagrams show, for simplification, an abrupt decomposition of the perovskites in reducing atmospheres, whereas it should be seen as a continuous change, as expressed by Fig. 3. Taking into account the non-stoichiometry, introduced by the reduction of the perovskite, did not modify much the stability diagrams of Ca- and Sr-substituted $LaCrO_3$.

Weight loss due to vaporization is normally considered important only if the vapour pressure of the evaporating species is higher than 10^{-8} atm [30]. This limit is presented on the volatility diagrams as a dotted horizontal line.

H_2O is observed to have a large effect on the stability of these perovskites, as seen from the increased volatility arising from hydroxy-volatile Cr, Ca and Sr compounds (dashed lines in Fig. 4). The volatility of the Ca- and Sr-substituted compounds are increased by eight orders of magnitude at middle P_{O_2} ranges of 10^{-20} atm. It is clearly seen that Ca is more volatile than Sr as the partial pressures for Ca hydroxyles are higher.

H_2 has a similar effect as shown in Fig. 4. In the absence of the thermodynamic data for the rare earth carbonates as well as for Cr, only Ca and Sr carbonates were considered. From that simplified approach, CO and CO_2 are expected to have almost no effect on the stability of these perovskites, as shown in the diagrams and as far as no carbon is formed and no secondary phases are present. The effect of the latter is given as:

$$SrCrO_3 + CO_2 = SrCO_3 + 0.5Cr_2O_3 + 0.25O_2;$$
$$\Delta G_{800\,^\circ C} = 10.8\,\text{kJ/mol} \quad (11)$$

$$SrCrO_4 + CO_2 = SrCO_3 + 0.5Cr_2O_3 + 0.75O_2;$$
$$\Delta G_{800\,^\circ C} = 23.5\,\text{kJ/mol} \quad (12)$$

$$Sr_2CrO_4 + 2CO_2 = 2SrCO_3 + 0.5Cr_2O_3 + 0.25O_2;$$
$$\Delta G_{800\,^\circ C} = 2.2\,\text{kJ/mol} \quad (13)$$

$$CaCrO_3 + CO_2 = CaCO_3 + 0.5Cr_2O_3 + 0.25O_2;$$
$$\Delta G_{800\,^\circ C} = 12.6\,\text{kJ/mol} \quad (14)$$

$$CaCrO_4 + CO_2 = CaCO_3 + 0.5Cr_2O_3 + 0.75O_2;$$
$$\Delta G_{800\,^\circ C} = 16.5\,\text{kJ/mol} \quad (15)$$

$$CaCr_2O_4 + CO_2 = CaCO_3 + Cr_2O_3;$$
$$\Delta G_{800\,^\circ C} = 13.1\,\text{kJ/mol} \quad (16)$$

These reaction—11, 12, 14 and 15—proceed at a P_{O_2} of 1.5×10^{-9}, 4.1×10^{-7}, 5.5×10^{-11} and 3.3×10^{-5} atm respectively. The effect of carbon was not analyzed (carbide formation, reducing agent). The meaning of all the lines shown in the diagrams are described in more details by Lou et al. [30,31].

3.5. Stability in low oxygen partial pressures (Mg, Mn, Fe, Co, Ni)

The lanthanum nickelate system is quite complicated showing a large variation in non-stoichiometry and composition [3,32,33]. This is also the case for the other transition metal lanthanum oxides studied here. For the stability calculations, only $LaNiO_3$, La_2NiO_4, $La_4Ni_3O_{10}$ and $LaCr_{1-x}Ni_xO_3$ were considered. Fig. 5 exposes the solubility limit of $LaCr_{1-x}Ni_xO_3$ as a function of temperature and oxygen partial pressure. As for Mg [10], Ca or Sr substitution, the solubility limit varies with the oxygen partial pressure. Ni substitution, *B*-site, is seen to be thermodynamically less favored than Ca, in reducing atmospheres.

Our thermodynamic calculations, limited to the very few compounds taken into account, indicate further that, at 850 °C, the Fe substituted lanthanum chromites would decompose at a P_{O_2} of 1.26×10^{-23}, to yield the metal and the $LaCrO_3$ phase, while with Mg, Ca, Sr, Mn and Co the LC should decompose to the metal oxide and $LaCrO_3$ phases at a P_{O_2} of 1.6×10^{-14}, 1.0×10^{-19}, 1.6×10^{-26},

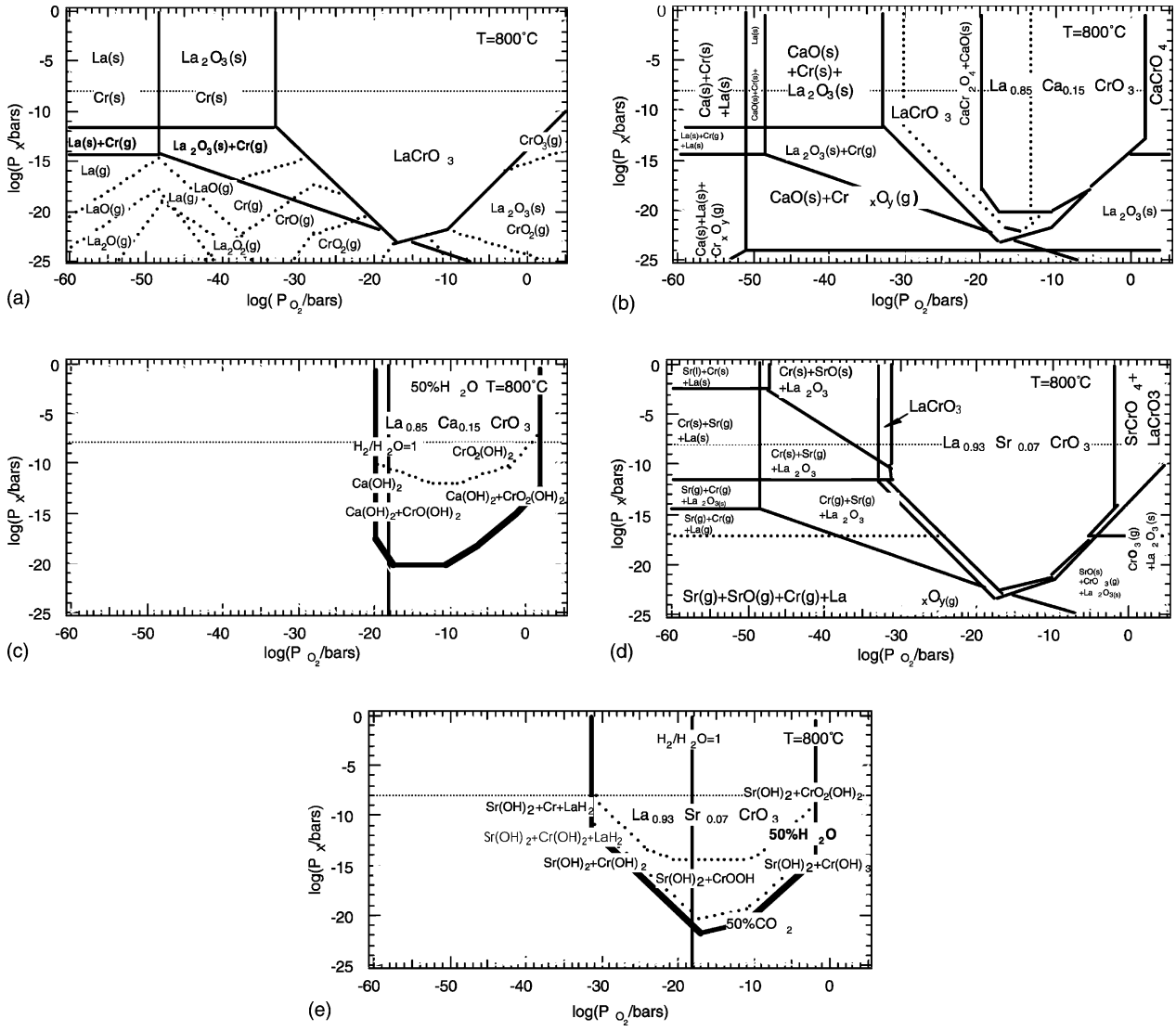

Fig. 4. Volatility diagrams for the $LaCrO_3$, $La_{0.85}Ca_{0.15}CrO_3$ and $La_{0.93}Sr_{0.07}CrO_3$ systems, at 800 °C. The effect of H_2O and CO_2 is also highlighted. H_2 has a similar effect to H_2O. The presence of impurities can modify much the secondary phases composition.

6.3×10^{-24} and 1.9×10^{-14} atm respectively. In these systems, no chemical thermodynamic analysis was undertaken in the perspective of understanding the effect of corrosive gases (air, wet hydrogen, CO and CO_2).

3.6. Interfacial reaction with YSZ

Beside Ni who may form mixed phases with YSZ [15], the pyrochlore phase, $La_2Zr_2O_7$, is the main reaction product of LaMO_3 with YSZ, M = Mg, Mn, Fe and Co [34]. From these thermodynamic calculations, $La_2Zr_2O_7$ does not form under SOFC conditions for Ca and Sr whereas (Ca, Sr)ZrO_3 is readily obtained. Sr-substituted $LaCrO_3$ is observed to be more stable toward these reactions. Ni forms readily $La_2Zr_2O_7$ as nickel zirconates are reported to be unstable [34]. These results indicate that the surface reactions between YSZ and the $LaCrO_3$ based anodes could be of importance, in reducing conditions, even at low temperatures. However, there is no experimental evidence (*SEM* analysis) that the anode itself reacted directly with YSZ, unless treated above 1100 °C or when heavily substituted [5].

At $x = 0.15$ of Ca- or Sr-, or $x = 0.1$ of Ni, substituted $LaCrO_3$ is not expected to react with YSZ at 1200 °C in air. $LaCrO_3$ is expected to be very stable toward YSZ, both in reducing and oxidizing conditions, unless Cr dissolves into YSZ [35] which would allow the resulting precipitated La_2O_3 to react with YSZ following reaction (18).

$$LaCrO_3 + ZrO_2 = 0.5La_2Zr_2O_7 + 0.5Cr_2O_3;$$
$$\Delta G_{850\,^\circ C} = 24.7\,\text{kJ/mol} \quad (17)$$

$$La_2O_3 + ZrO_2 = 0.5La_2Zr_2O_7;$$
$$\Delta G_{850\,^\circ C} = -52.6\,\text{kJ/mol} \quad (18)$$

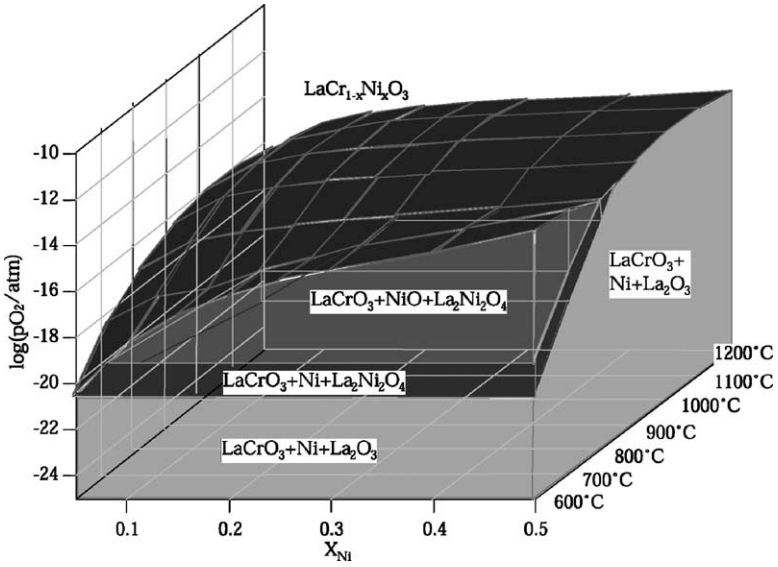

Fig. 5. Estimated solubility limit of $LaCr_{1-x}Ni_xO_3$. The solubility is a function of P_{O_2} as in the case of $LaCr_{1-x}Mg_xO_3$ [10]. In these calculations, the non-stoichiometry was not taken into account.

4. Discussion

Correlation of these calculations with experimental results is possible. The volatility diagrams show that the surrounding gas phase in equilibrium at different P_{O_2} with $LaCrO_3$ is essentially made up of CrO_3(g), CrO_2(g), Cr(g) and LaO(g) (see Fig. 4, case of $LaCrO_3$). This agrees well with measurements made at 1600 °C by Peck et al. [36].

The changes in composition of the chromium gas phase as a function of oxygen partial pressure are also well predicted in our diagrams when compared to the reported one at 950 °C by Hilpert et al. [37]. Similarily, as shown in Fig. 4, $CrO_2(OH)_2$(g) is predicted to be the dominant Cr gaseous species in humidified atmospheres, in accordance with literature [37]. Also, the secondary phase for the Ca-substitution is predicted to be $CaCr_2O_4$ in reducing atmospheres in accordance with Peck et al. [21].

XPS measurements made on $x = 0.15$ for Ca- and Sr-substituted $LaCrO_3$ show a small excess of these elements on the surface of freshly prepared samples (see Table 1). This could stem from the preparation procedure [7]. It was previously observed that a calcination temperature of at least 1100 °C was necessary to produce an *XRD* pure perovskite. However, as reported in literature, pure substituted $LaCrO_3$ has a very narrow window and secondary phases beneath *XRD* detection level would be always expected [7,11,27]. Also, the slow cooling of the calcined powder could also cause a demixing of Ca or Sr rich compounds, as the solubility limit is low at room temperature, as discussed above. Another explanation could be the melts responsible of the sintering of the $LaCrO_3$-based compounds which are left on the surface of the perovskites as very thin layers [6].

Table 1 also shows a surface enrichment of the perovskites with Ca or Sr substitution upon treatment in reducing atmospheres. It is clearly seen that, for runs of 100 h, wet hydrogen had an effect on the segregation, whereas air or CO_2 did not affect the system much (the three last lines in Table 1). Ca is seen to segregate more readily than Sr and this could be eventually explained by the lower stability limit in H_2 or the higher volatility of Ca, as discussed above. Cr, on the other hand, did not segregate as the La/Cr ratio did not change much after catalysis.

Ni substitution, *B*-site, is seen to be thermodynamically less favored than Ca, in reducing atmospheres. However, *XRD* measurements made on a $LaCr_{0.5}Ni_{0.5}O_3$ powder, exposed for 1 week at 780 °C to $H_2 + 3\%$ H_2O showed no demixing.

Also, our catalytic runs in 3% $H_2O + CH_4$ and in 5:1 CH_4:O_2 on $LaCr_{0.9}Ni_{0.1}O_3$ and $La_{0.85}Ca_{0.15}Cr_{0.9}Ni_{0.1}O_3$ powders did not cause any phase segregation [7]. This indicates that the decomposition of the Ni-substituted $LaCrO_3$ is kinetically hindered. The same has been previously observed in literature for another (Mg) *B*-site substituted $LaCrO_3$ [10].

Mg, Mn, Fe and Co did not segregate further after the catalytic runs (see Table 1), indicating that they may not destabilize the perovskite structure. This is in accordance with experimental temperature programmed reduction (*TPR*) results [7], which showed clearly that all of the lanthanum chromite catalysts did not undergo total reduction of the *B*-site substituent. Our experimental results suggest that the decomposition of these materials is hindered kinetically.

Experimentally, CaO and calcium oxychromates, $Ca_m(CrO_4)_n$, exsoluted from a $La_{0.7}Ca_{0.32}CrO_3$ anode were observed to react readily with YSZ at 900 °C to form

Table 1
Summary of the XPS surface analysis given in percent of the sum of the total metal elements

XPS analysis (%) catalyst composition	La/Cr	Mg	Ca	Sr	Mn	Fe	Co	Ni[a]	Ca, Sr nominal	Mg, Mn, Fe, Co, Ni nominal
$LaCrO_3$, ap	0.9									
$LaCr_{0.9}Mg_{0.1}O_3$, ap	2.9	5.3								5
$LaCr_{0.9}Mg_{0.1}O_3$, ac	2.8	4.9								5
$La_{0.85}Ca_{0.15}CrO_3$, ap	1.0		10						7.5	
$La_{0.85}Ca_{0.15}CrO_3$, ac	1.0		22						7.5	
$La_{0.7}Ca_{0.32}CrO_3$, ap	1.0		39						16	
$La_{0.85}Sr_{0.15}CrO_3$, ap	0.9			10					7.5	
$La_{0.85}Sr_{0.15}CrO_3$, ac	0.8			14					7.5	
$LaCr_{0.9}Mn_{0.1}O_3$, ap	1.2				5					5
$LaCr_{0.9}Mn_{0.1}O_3$, ac	1.3				5.7					5
$LaCr_{0.9}Fe_{0.1}O_3$, ap	1.1					7.3				5
$LaCr_{0.9}Fe_{0.1}O_3$, ac	1.2					8.7				5
$LaCr_{0.9}Co_{0.1}O_3$, ap	1.2						1.9			5
$LaCr_{0.9}Co_{0.1}O_3$, ac	1.3						2.8			5
$LaCr_{0.9}Ni_{0.1}O_3$, ap	1.6							?		5
$LaCr_{0.9}Ni_{0.1}O_3$, ac	1.9							?		5
$La_{0.85}Ca_{0.15}Cr_{0.9}Ni_{0.1}O_3$, ap	1.0		10					?	7.5	5
$La_{0.85}Ca_{0.15}Cr_{0.9}Ni_{0.1}O_3$, ac	0.8		21					?	7.5	5
$La_{0.85}Ca_{0.15}Cr_{0.9}Ni_{0.1}O_3$, H_2	1.2		15					?	7.5	5
$La_{0.85}Ca_{0.15}Cr_{0.9}Ni_{0.1}O_3$, CO_2	1.0		9					?	7.5	5
$La_{0.85}Ca_{0.15}Cr_{0.9}Ni_{0.1}O_3$, air	1.2		6					?	7.5	5

ap: as prepared; ac: after catalysis with CH_4. The last three lines show the influence of some gases on the surface segregation [7].
[a] Ni peak could not be resolved because of overlapping with La 3d peaks.

$CaZrO_3$ as assessed from impedance spectroscopy [5] and *XPS-Auger-SIMS* analysis [5]. The $CaZrO_3$ or $SrZrO_3$ formation could be attribsuted to some of the following reactions:

$$CaO + ZrO_2 = CaZrO_3; \quad \Delta G_{850\,^\circ C} = -47.5\,kJ/mol \tag{19}$$

$$CaCrO_4 + ZrO_2 = CaZrO_3 + 0.5Cr_2O_3 + 0.75O_2; \quad \Delta G_{850\,^\circ C} = 32.1\,kJ/mol \tag{20}$$

$$CaCrO_3 + ZrO_2 = CaZrO_3 + 0.5Cr_2O_3 + 0.25O_2; \quad \Delta G_{850\,^\circ C} = 17.4\,kJ/mol \tag{21}$$

$$CaCr_2O_4 + ZrO_2 = CaZrO_3 + Cr_2O_3; \quad \Delta G_{850\,^\circ C} = 20.5\,kJ/mol \tag{22}$$

$$SrO + ZrO_2 = SrZrO_3; \quad \Delta G_{850\,^\circ C} = -90.1\,kJ/mol \tag{23}$$

$$SrCrO_3 + ZrO_2 = SrZrO_3 + 0.5Cr_2O_3 + 0.25O_2; \quad \Delta G_{850\,^\circ C} = 19.7\,kJ/mol \tag{24}$$

$$SrCrO_4 + ZrO_2 = SrZrO_3 + 0.5Cr_2O_3 + 0.75O_2; \quad \Delta G_{850\,^\circ C} = 56.3\,kJ/mol \tag{25}$$

$$Sr_2CrO_4 + ZrO_2 = SrZrO_3 + 0.5Cr_2O_3 + SrO + 0.25O_2; \quad \Delta G_{850\,^\circ C} = 24.2\,kJ/mol \tag{26}$$

$$Sr_2CrO_4 + 2ZrO_2 = 2SrZrO_3 + 0.5Cr_2O_3 + 0.25O_2; \quad \Delta G_{850\,^\circ C} = -65.8\,kJ/mol \tag{27}$$

These reactions—20, 21, 23, 25, 26 and 27—are already favorable below a P_{O_2} of 2.6×10^{-5} atm at 850 °C. This indicates clearly that secondary phases could play an important role in the anode degradation, and thus should be minimized.

4.1. Kinetically limited decomposition?

In literature, measurements done on cation tracer bulk diffusion in $LaCrO_3$-based materials showed that Cr diffusion is slower than La, Ca and Sr diffusion by one to two orders of magnitude [38–42] (see Table 2). This might also explain the differences, after catalysis, in surface composition between *A*-site- and *B*-site-substituted $LaCrO_3$. Tracer grain boundary diffusion coefficients are also higher for Ca and Sr than for Cr by about two orders of magnitude [41]. In both cases Ca diffusion is faster than Sr diffusion [39]. This could also explain the difference in the segregation. The effect of P_{O_2} on the cation diffusion coefficients is not very clear [39,40]. However, in air, the tracer grain boundary diffusion coefficients for the cations and the anion are of the same order of magnitude.

Also, as previously observed [5,6], current induced the demixing of Ca/Sr-rich substituted $LaCrO_3$ leading to the deposition of a 1 nm thick Ca/Sr rich layer over porous anode structures. As the Ca grain boundary diffusion coefficient is of the same magnitude as the oxygen anions grain boundary diffusion coefficient (Table 2), the presence of a potential gradient or the flow of a current in the $LaCrO_3$-based anode might then have an effect on the migration of

Table 2
Tracer bulk diffusion and grain boundary diffusion coefficients (D_{bulk}, $D_{g.b.}$), at 1000 °C, and their activation energies, taken from [38–42]

Compound	Level of substitution	Element diffusing	D_{bulk} (m^2/s)	E_a (kJ/mol)	$D_{g.b.}$ (m^2/s)	E_a (kJ/mol)
LCC	Ca 0.25	Cr	1.07×10^{-21}	213	$1.57x10^{-15}$	266
	Ca 0.3	O	2.2×10^{-16}	–	2×10^{-11} to 6×10^{-15}	–
	Ca 0.25	Ca	10^{-19}	222	10^{-13} to 10^{-12}	192
LC		La	$10^{-19.75}$	482	–	–

these cations on the surface of the anode grains. Their migration would proceed in the opposite direction to the electrons and oxygen anions, leading to their segregation on the anode/YSZ interface, and ultimately to an interfacial reaction with the electrolyte.

5. Conclusions

$LaCrO_3$-based compounds' stability was assessed, based on thermodynamic as well as experimental results. It was found that on the *A*-site, Sr substitution is more favorable than Ca in reducing atmospheres. H_2O and H_2 are expected to corrode the perovskites, as the volatility of the Ca, Sr and Cr are more pronounced due to the formation of hydroxy-species. Furthermore, the higher the substitution with Ca or Sr the larger the destabilization of the perovskite, both in air and in reducing atmospheres—the $LaCrO_3$ seems to accommodate more Sr in reducing atmospheres. The secondary phases formed during the decomposition could react readily with YSZ at 800 °C, as observed experimentally. Overall, the $LaCrO_3$ are thermodynamically quite reactive toward YSZ but this was not observed experimentally unless treated above 1100 °C. Also, Mg, Mn, Fe, Co and Ni, *B*-site-substituted compounds, although thermodynamically unstable, are quite stable experimentally suggesting that the decomposition of *B*-site substituted lanthanum chromites is hindered kinetically. The *A*-site substitution seems to be more problematic.

Acknowledgements

The present author is grateful to Dr. Harumi Yokokawa, from NIMC, Japan, Dr. Leila Grahl-Madsen from IRD, Denmark, and Prof. Klaus Hilpert, from Research Center Jülich, Germany, for providing the thermodynamic data of some compounds. Many thanks are due to Prof. P. A. Buffat, Dr. P. Möckli, Dr. D. Léonard and Mr. N. Xanthopoulos, all members of the Department of Materials Science at EPFL, for experimental surface analysis and powder characterizations. The financial support of the Japanese NEDO 98-EF2 project is also acknowledged. This paper is taken from a chapter of the Ph.D. thesis of J. Sfeir, 'Alternative anode materials for methane oxidation in solid oxide fuel cells', EPFL thesis No. 2446 (2001).

Appendix A. List of the species taken into account for the calculations:

- $H_2(g)$, $H_2O(g)$, $O_2(g)$, Ar(g), CO(g), $CO_2(g)$,
- Cr(s), Cr(g), CrOH(g), CrO(g), $Cr(OH)_2(g)$, $Cr_2O_3(s)$, $Cr(OH)_3(g)$, CrOOH(g), $CrO_2(g)$, $Cr(OH)_3(g)$, $CrO(OH)_2(g)$, $CrO(OH)_3(g)$, $Cr(OH)_5(g)$, $CrO(OH)_3(g)$, $CrO_2OH(g)$, $CrO_3(g)$, $Cr(OH)_6(g)$, $CrO(OH)_4(g)$, $CrO_2(OH)_2(g)$,
- La(s), La(g), $LaH_2(s)$, $La_2O(g)$, LaO(g), $La_2O_2(g)$, $La_2O_3(s)$, $LaO_2(g)$,
- Mg(s), MgO(s),
- Ca(s), CaO(s), CaH(g), $CaH_2(s)$, CaOH(g), $Ca(OH)_2(g)$, $CaCO_3(s)$, $CaCrO_3(s)$, $CaCrO_4(s)$, $CaCr_2O_4(s)$, $Ca_2CrO_4(s)$, $Ca_3Cr_2O_7(s)$, $Ca_3Cr_2O_8(s)$, $Ca_5(CrO_4)_3(s)$, $Ca_5(CrO_3)_4O(s)$, $Ca_{10}(CrO_4)_7(s)$,
- Sr(l), Sr(g), SrH(g), SrOH(g), SrO(s), $Sr(OH)_2(l)$, $Sr(OH)_2(g)$, $SrCO_3(s)$, $SrCrO_3(s)$, $SrCrO_4(s)$, $Sr_2CrO_4(s)$, $Sr_3Cr_2O_8(s)$,
- Mn(s), MnO(s), $Mn_2O_3(s)$, $Mn_3O_4(s)$,
- Fe(s), FeO(s), $Fe_2O_3(s)$, $Fe_3O_4(s)$, $FeCr_2O_4(s)$,
- Co(s), CoO(s), $Co_2O_3(s)$, $CoCr_2O_4(s)$,
- Ni(s), NiO(s), $Ni_2O_3(s)$, $NiCr_2O_4(s)$,
- Cu(s), CuO(s),
- Zn(s), ZnO(s),
- $La_2CrO_4(s)$, $La_2CrO_6(s)$, $La_2(CrO_4)_3(s)$, $LaCrO_4(s)$, $LaCr_{1-x}Mg_xO_3(s)$, $LaCaCrO_4(s)$, $LaCa_2Cr_2O_7(s)$, $La_3Ca_2O_7(s)$, $La_{1-x}Ca_xCrO_3(s)$, $La_{1-x}Ca_xCrO_{3-\delta}(s)$, $LaSrCrO_4(s)$, $La_{1-x}Sr_xCrO_3(s)$, $La_{1-x}Sr_xCrO_{2-\delta}(s)$, $LaCr_{1-x}Mn_xO_3(s)$, $LaCr_{1-x}Fe_xO_3(s)$, $LaCr_{1-x}Co_xO_3(s)$, $LaNiO_3(s)$, $La_2NiO_4(s)$, $La_4Ni_3O_{10}(s)$, $LaCr_{1-x}Ni_xO_3(s)$, $LaCr_{1-x}Cu_xO_3(s)$, $LaCr_{1-x}Zn_xO_3(s)$,
- $ZrO_2(s)$, $CaZrO_3(s)$, $SrZrO_3(s)$, $La_2Zr_2O_7(s)$, $La_2NiZrO_4(s)$, $La_4Ni_2ZrO_{10}(s)$

Appendix B. Generated thermodynamic parameters for the compounds of the substituted LaCrO3 phases. The heat capacity is given as C_p (kJ/mol$K$) $= A + B10^{-3}T + C10^{5}T^{-2} + D10^{-6}T^{2}$, with T in Kelvin

Compounds	$\Delta_f H^{\circ}_{298}$ (kJ/mol)	S°_{298} (J/mol K)	A	B	C	D
$LaCrO_3$	−1534.40	114.00	119.30	12.05	−14.64	0.00
$La_{0.5}Ca_{0.5}CrO_3$	−1420.51	106.69	128.10	20.51	−4.95	−0.95
$La_{0.5}Ca_{0.5}CrO_{2.75}$	−1201.35	101.47	106.9	18.04	−3.05	−1.90
$La_{0.5}Sr_{0.5}CrO_3$	−1416.21	115.41	126.06	25.77	−3.37	−3.03
$La_{0.5}Sr_{0.5}CrO_{2.75}$	−1173.24	110.19	104.9	23.31	−1.47	−3.98
$LaCr_{0.5}Mg_{0.5}O_3$	−1546.07	112.64	131.08	17.97	−12.18	−0.13
$LaCr_{0.5}Mg_{0.5}O_{2.75}$	−1521.42	107.42	109.88	15.51	−10.29	−1.08
$LaCr_{0.5}Mn_{0.5}O_3$	−1483.34	121.57	111.81	21.99	−8.23	−0.95
$LaCr_{0.5}Mn_{0.5}O_{2.75}$	−1421.56	123.81	109.19	17.28	−6.70	−0.95
$LaCr_{0.5}Fe_{0.5}O_3$	−1455.40	115.81	110.51	32.68	−8.57	−0.95
$LaCr_{0.5}Fe_{0.5}O_{2.75}$	−1372.62	122.75	111.34	17.53	−6.51	−0.95
$LaCr_{0.5}Co_{0.5}O_3$	−1314.66	118.62	111.16	27.34	−8.40	−0.95
$LaCr_{0.5}Co_{0.5}O_{2.75}$	−1351.23	120.44	111.61	13.36	−3.46	1.22
$LaCr_{0.5}Ni_{0.5}O_3$	−1370.03	118.18	270.06	−508.55	−38.60	577.77
$LaCr_{0.5}Ni_{0.5}O_{2.75}$	−1209.77	112.95	248.85	−511.02	−36.70	576.8
$LaCr_{0.5}Cu_{0.5}O_3$	−1321.82	120.48	131.44	19.40	−10.56	0.00
$LaCr_{0.5}Cu_{0.5}O_{2.75}$	−1161.77	115.78	110.24	16.94	−8.66	−0.95
$LaCr_{0.5}Zn_{0.5}O_3$	−1415.73	121.00	129.82	19.33	−9.61	0.00
$LaCr_{0.5}Zn_{0.5}O_{2.75}$	−1255.78	112.95	108.62	16.87	−7.71	−0.95

References

[1] M. Mori, N. Sakai, T. Kawada, H. Yokokawa, M. Dokya, A new cathode material (La, Sr)$_{1-z}$($Mn_{1-y}Cr_y$)O_3 ($0 \le y \le 0.2$) for SOFC, Denki Kagaku 58 (1990) 528–532.

[2] T. Norby et al., Oxidation of CH_4 on $La_{0.7}Ca_{0.3}CrO_3$/YSZ anodes, in: U. Bossel (Ed.), Proceedings of the European Solid Oxide Fuel Cell Forum I, Ulf Bossel, Lucerne, Switzerland, 1994, pp. 217–226.

[3] T. Nakamura, G. Petzow, L.J. Gauckler, Stability of perovskite phase $LaBO_3$ (B = V, Cr, Mn, Fe, Co, Ni) in reduced atmosphere. I. Experimental results, Mat. Res. Bull. 14 (1979) 649–659.

[4] L.G. Tejuca, J.L.G. Fierro, J.M.D. Tascon, Structure and reactivity of perovskite-type oxides, Adv. Catal. 36 (1989) 237–328.

[5] J. Sfeir, J. Van herle, A.J. McEvoy, $LaCrO_3$ based anodes for methane oxidation, in: P. Stevens (Ed.), Proceedings of the Third European Solid Oxide Fuel Cell Forum, Ulf Bossel, Nantes-France, 1998, pp. 267–276.

[6] J. Sfeir, J. Van herle, A.J. McEvoy, Stability of calcium substituted lanthanum chromites used as SOFC anodes for methane oxidation, J. Euro. Ceramic Soc. 19 (1999) 897–902.

[7] J. Sfeir et al., Lanthanum chromite based catalysts for oxidation of methane directly on SOFC anodes, J. Catal. 202 (2001) 229–244.

[8] J. Sfeir, R. Vasquez, J. Van herle, in: J. Huijsmns (Ed.), Proceedings of the Fifth European Solid Oxide Fuel Cell Forum, Ulf Bossel, Lucerne, Switzerland, 2002, pp. 570–577.

[9] H. Yokokawa, N. Sakai, T. Kawada, M. Dokiya, Chemical thermodynamic considerations in sintering of $LaCrO_3$-based perovskites, J. Electrochem. Soc. 138 (1991) 1018–1027.

[10] V. Van. Dieten, Electrochemical vapour deposition of SOFC interconnection materials, Ph.D. thesis, Technische Universiteit Delft, 1995.

[11] H. Yokokawa, N. Sakai, T. Kawada, M. Dokiya, Thermodynamic stabilities of perovskite oxides for electrodes and other electrochemical materials, Solid State Ionics 52 (1992) 43–56.

[12] R.D. Shannon, C.T. Prewitt, Effective ionic radii in oxides and fluorides, Acta Cryst. B25 (1969) 925–946.

[13] I. Yasuda, M. Hishinuma, Electrochemical properties of doped lanthanum chromites as interconnectors for solid oxide fuel cells, J. Electrochem. Soc. 143 (1996) 1583–1590.

[14] D.H. Peck, K. Hilpert, M. Miller, D. Korbertz, H. Nickel, Forschungszentrum Jülich GmbH, Institut für Werkstoffe der Energietechnik, 1996.

[15] H. Yokokawa, N. Sakai, T. Kawada, M. Dokiya, Thermodynamic analysis of reaction profiles between $LaMnO_3$ (M = Ni, Co, Mn) and ZrO_2, J. Electrochem. Soc. 138 (1991) 2719–2727.

[16] I. Yasuda, M. Hishinuma, Electrical conductivity and chemical stability of calcium chromate hydroxyl apatite, $Ca_5(CrO_4)_3OH$, and problems caused by the apatite formation at the electrode/separator interface interface in solid oxide fuel cells, Solid State Ionics 78 (1995) 109–114.

[17] N. Sakai, T. Kawada, H. Yokokawa, M. Dokiya, I. Kojima, Liquid-phase-assisted sintering of calcium-doped lanthanum chromites, J. Am. Ceram. Soc. 76 (1993) 609–616.

[18] N. Sakai, T. Kawada, H. Yokokawa, M. Dokiya, Effect of preparation method on chemical stability of sinterable calcium doped lanthanum chromites, J. Ceramic Soc. Jpn. 101 (1993) 1195–1200.

[19] H. Yokokawa et al., Simultaneous thermogravimetry-mass spectroscopy for a solid oxide fuel cell interconnect, $(La_{0.7}Ca_{0.32})CrO_3$, Thermochim. Acta 267 (1995) 129–138.

[20] D.H. Peck, M. Miller, K. Hilpert, Phase diagram studies in the SrO–Cr_2O_3–La_2O_3 system in air and under low oxygen pressure, Solid State Ionics 123 (1999) 59–65.

[21] D.H. Peck, M. Miller, K. Hilpert, Phase diagram study in the CaO–Cr_2O_3–La_2O_3 system in air and under low oxygen pressure, Solid State Ionics 123 (1999) 47–57.

[22] D.H. Peck, M. Miller, H. Nickel, D. Das, K. Hilpert, The SrO-Cr_2O_3-La_2O_3 phase diagram and volatility of $La_{1-x}Sr_xCrO_3$ (x = 0–0.3) in comparison to Cr base interconnect alloys, in: M. Dokiya,

O. Yamamoto, H. Tagawa, S.C. Singhal (Eds.), Proceedings of the Fourth International Symposium on Solid Oxide Fuel Cells, The Electrochemical Society, 1995, pp. 858–868.

[23] S. Miyoshi et al., Solubility limit of alkaline earth oxide in lanthanum chromite, in: A.J. McEvoy (Ed.), Proceedings of the Forth European Solid Oxide Fuel Cell Forum, Lucerne, Switzerland, 2000, pp. 881–887.

[24] L.A. Chick, J.L. Bates, G.D. Maupin, in: F. Grosz, P. Zegers, S.C. Singhal, O. Yamamoto (Eds.), Proceedings of the Second International Symposium on Solid Oxide Fuel Cells, Commission of the European Communities, Directorate-General, Telecommunications, Information Industries and Innovation, Athens, Greece, 1991, pp. 621–628.

[25] J.D. Carter, V. Sprenkle, M.M. Nasrallah, H.U. Anderson, Solubility of calcium in lanthanum chromite, in: S.C. Singhal, H.I. (Eds.), Proceedings of the Third International Symposium on Solid Oxide Fuel Cells, The Electrochemical Society Inc., NJ, Honolulu, Hawaii, 1993, pp. 344–353.

[26] R.W. Berg, in: F.W. Poulsen, N. Bonanos, S. Linderoth, M. Mogensen, B. Zachau-Christiansen (Eds.), High Temperature Electrochemistry: Ceramics and Metals, Risø National Laboratory, Roskilde, Denmark, Risø National Laboratory, Roskilde, Denmark, 1996, pp. 175–180.

[27] L.A. Chick et al., Phase transitions and transient liquid-phase sintering in calcium-substituted lanthanum chromite, J. Am. Ceram. Soc. 80 (1997) 2109–2120.

[28] B.J. Wood, D.G. Fraser, Elementary Thermodynamics for Geologists, Oxford University Press, 1976.

[29] H.A.J. Oonk, Phase Theory. The Thermodynamics of Heterogeneous Equilibria, Elsevier, 1981.

[30] V.L.K. Lou, T.E. Mitchell, A.H. Heuer, Review—graphical displays of the thermodynamics of high-temperature gas–solid reactions and their application to oxidation of metals and evaporation of oxides, J. Am. Ceram. Soc. 68 (1985) 49–58.

[31] V.L.K. Lou, A.H. Heuer, in: R.J. Fordham (Ed.), High Temperatures–High Pressures, Elsevier, Petten, The Netherlands, 1990, pp. 33–52.

[32] T. Moriga et al., Characterization of oxygen-deficient phases appearing in reduction of the perovskite-type $LaNiO_3$ to $La_2Ni_2O_5$, Solid State Ionics 79 (1995) 252–255.

[33] H.E. Höfer, W.F. Kock, Crystal chemistry and thermal behaviour in the La(Cr, Ni)O_3 perovskite system, J. Electrochem. Soc. 140 (1993) 2889–2894.

[34] H. Yokokawa, N. Sakai, T. Kawada, M. Dokiya, Phase diagram calculations for ZrO_2 based ceramics: thermodynamic regularities in zirconate formation and solubilities of transition metal oxides, in: S.P.S. Badwal, M.J. Bannister, R.H. Hannink (Eds.), Science and Technology of Zirconia, 1993, pp. 59–68.

[35] H. Yokokawa, N. Sakai, T. Kawada, M. Dokiya, Chemical thermodynamic compatibility of solid oxide fuel cell materials, in: F. Grosz, P. Zegers, S.C. Singhal, O. Yamamoto (Eds.), Proceedings of the Second International Symposium on Solid Oxide Fuel Cells, Commission of the European Communities, Directorate-General, Telecommunications, Information Industries and Innovation, Athens, Greece, 1991, pp. 663–670.

[36] D.H. Peck, M. Miller, D. Kobertz, H. Nickel, K. Hilpert, Vaporization of $LaCrO_3$: partial and integral thermodynamic properties, J. Am. Ceram. Soc. 79 (1996) 3266–3272.

[37] K. Hilpert, D. Das, M. Miller, D.H. Peck, R. Weiß, Chromium vapor species over solid oxide fuel cell interconnect materials and their potential for degradation processes, J. Electrochem. Soc. 143 (1996) 3642–3647.

[38] T. Kawada, T. Horita, N. Sakai, H. Yokokawa, M. Dokiya, Experimental determination of oxygen permeation flux through bulk and grain boundary of $La_{0.7}Ca_{0.3}CrO_3$, Solid State Ionics 79 (1995) 201–207.

[39] T. Horita et al., Cation diffusion in (La, Ca)CrO_3 perovskite by SIMS, Solid State Ionics 108 (1995) 383–390.

[40] T. Horita, Calcium tracer diffusion in (La, Ca)CrO_3 by SIMS, Solid State Ionics 124 (1999) 301–307.

[41] N. Sakai, K. Yamaji, T. Horita, H. Negishi, H. Yokokawa, Chromium diffusion in lanthanum chromites, Solid State Ionics 135 (2000) 469–474.

[42] T. Akashi, M. Nanko, T. Maruyama, Y. Shiraishi, J. Tanabe, Diffusion coefficient of La^{3+} in $LaCrO_3$ determined by solid state reaction, in: U. Stimming, S.C. Singhal, H. Tagawa, W. Lehnert (Eds.), Solid Oxide Fuel Cells V, The Electrochemical Society, Aachen, Germany, 1997, pp. 1263–1272.